Continuum Mech. Thermodyn.
https://doi.org/10.1007/s00161-024-01303-6

ORIGINAL ARTICLE

František Maršík · Zdeněk Trávníček · Bernhard Weigand · Florian Seibold · Zuzana Antošová

Swirl flow stability: thermodynamic analysis and experiments

Received: 4 April 2023 / Accepted: 7 April 2024
© The Author(s) 2024

Abstract The current paper presents a theoretical analysis of swirl flow stability, both inside a tube (vortex tube) and in a free annular swirl flow. The starting concept is the study of the evolution of velocity and temperature fluctuations. Methods of non-equilibrium thermodynamics are used to describe the magnitude of fluctuations and their properties. The important role of the total enthalpy follows from a variational analysis. Moreover, the thermodynamic criterion of the stability is formulated using the total enthalpy, and compared with experiments, numerical results and classical Rayleigh theory support its applicability. It was shown that the solid body vortex is at the margin of stability, which is experimentally observed. Analogously, the potential vortex is by the thermodynamic criterion stable; however, by the Rayleigh criteria it is on the onset of stability. The classical Taylor experiment of flow between two rotating cylinders is analysed from the point of view of this criterion. These results are underlined by swirl tube experiments at the Institute of Aerospace Thermodynamics at Stuttgart University and the annular nozzle experiments performed in the Institute of Thermomechanics CAS in Prague. Both independent experiments confirm the transformation of the initial annular vortex into a stable potential-type vortex. The results of this theory can also be used to explain the exceptional stability of tropical cyclones.

Keywords Thermodynamic stability condition · Annular swirl flow · Vortex tube · Tropical cyclone

František Maršík, Zdeněk Trávníček, Bernhard Weigand, Florian Seibold and Zuzana Antošová have contributed equally to this work.

F. Maršík · Z. Trávníček (✉) · Z. Antošová
Thermodynamics, Institute of Thermomechanics CAS, Dolejškova 5, 18200 Prague, Czech Republic
E-mail: tr@it.cas.cz

F. Maršík
E-mail: marsik@it.cas.cz

Z. Antošová
E-mail: antosova@it.cas.cz

B. Weigand · F. Seibold
Institute of Aerospace Thermodynamics (ITLR), University of Stuttgart, Pfaffenwaldring 31, 705 69 Stuttgart, Germany
E-mail: bernhard.weigand@itlr.uni-stuttgart.de

F. Seibold
E-mail: florian.seibold@itlr.uni-stuttgart.de

Published online: 10 May 2024

List of symbols

A	Cross-sectional area m^2
$A,\ B$	Couette flow parameters –
c	Speed of sound $\mathrm{m\,s}^{-1}$
c_p	Heat capacity at constant pressure $\mathrm{J\,kg}^{-1}\,\mathrm{K}^{-1}$
D	Tube diameter m
g	Gravitational acceleration $\mathrm{m\,s}^{-2}$
h	Specific enthalpy J kg
$h_\mathrm{lv} = h_\mathrm{vl}$	Evaporation/condensation heat $\mathrm{J\,kg}^{-1}$
L	Tube length, temperature slope $\mathrm{m},\ \mathrm{K\,m}^{-1}$
$\dot{m}$	Mass flow rate $\mathrm{kg\,s}^{-1}$
M	Molecular mass $\mathrm{kg\,mol}^{-1}$
p	Thermodynamic (static) pressure Pa
$\mathbf{q},\ q^i$	Heat flux $\mathrm{J\,m}^{-2}\,\mathrm{s}^{-1}$
$R_1,\ R_2$	Inner and outer cylinder radius m
Re	Reynolds number –
S	Swirl number –
s	Specific entropy $\mathrm{J\,kg}^{-1}\,\mathrm{K}^{-1}$
$\mathbf{t}_\mathrm{dis},\ t^{ij}_\mathrm{dis}$	Stress tensor, dissipative part Pa
T	Temperature K
t	Time s
u	Specific internal energy J kg
u_i	Velocity fluctuation $\mathrm{m\,s}^{-1}$
V	Average velocity $\mathrm{m\,s}^{-1}$
$\mathbf{v},\ v_i,\ v_\mathrm{r},\ v_\varphi,\ v_\mathrm{z}$	Velocity, velocity components $\mathrm{m\,s}^{-1}$
w	Mass concentration -
$x = \rho_\mathrm{v}/\rho_\mathrm{a}$	Vapour concentration -
$\mathbf{x},\ x^i,\ r,\ r\varphi,\ z$	Coordinates m

Greek symbols

β	Vertical velocity coefficient m^{-1}
δ	Fluctuation –
Γ	Circulation $\mathrm{m}^2\,\mathrm{s}^{-1}$
λ	Thermal conductivity $W\,m^{-1}\,K^{-1}$
ϵ	Turbulent dissipation $\mathrm{m}^2\,\mathrm{s}^{-3}$
$\eta = R_1/R_2$	Couette geometrical parameter –
$\mu,\ \mu = \Omega_2/\Omega_1$	Dynamic viscosity, Couette flow parameter $\mathrm{Pa\,s},\ -$
ν	Kinematic viscosity $\mathrm{m}^2\,\mathrm{s}^{-1}$
$\pi,\ \tilde{\pi}$	Dissipated energy density $\mathrm{J\,m}^{-3}\,\mathrm{s}^{-1}$
ρ	Density $\mathrm{kg\,m}^{-3}$
ϕ	Gravity potential, relative humidity $\mathrm{J\,kg}^{-1},\ -$
$\omega,\ \Omega$	Angular velocity s^{-1}

Indexes

0	Reference state,
a	Air
i, j, k, x, y, z	Cartesian components
mol	Molecular
r, φ, z	Cylindrical components
sat	Saturation
t	Total
v	Vapour
w	Wall

Superscripts

$(\dot{a})$, $\dot{\overline{\mathrm{da}}}$ Material derivative $\quad \dot{a}(\mathbf{x},t) = \frac{\partial a}{\partial t} + v^l \frac{\partial a}{\partial x^l}$

The Einstein summation rule is used, i.e. $v^l \frac{\partial a}{\partial x^l} = \sum_{l=1}^{l=3} v^l \frac{\partial a}{\partial x^l}$

1 Introduction

Despite a large number of experimental and theoretical results, the problem of stability of flow containing vortices is still open [5,17,25]. Important are some specific technical problems, e.g. the onset of turbulence in boundary layers on an airfoil, in pipes (especially in hose pipes, where the fluid–structure interaction has to be included) and especially the onset of the instability of swirl flows in pipes [21]. The problem is to find a suitable relationship between the magnitude of the velocity and the magnitude of the viscosity-induced velocity gradient even for flow along curved surfaces or in channels and pipes. In addition to experimental research, it is necessary to use very complex numerical simulations [6]. Also not fully understood is the flow stability with phase transition. Phase transition like condensation, evaporation, freezing takes a decisive role in atmospheric flow stability. Many open questions appear in biological flows where flow pulsations play a decisive role, for example, blood flow in arteries, bridging veins in the brain, etc. The understanding of the flow stability scenario is becoming highly important for practical engineering applications—in particular the applications involving heat transfer between fluid and solid walls, where it provides cues for the ever present endeavour to increase the transfer intensity. There are good chances to enhance the heat transfer from the walls of cooling channels by appropriate regulation of the cooling fluid flow parameters and by the design of the channel geometry [9,25]. Moreover, the instability leads to intensive fluid mixing resulting in higher intensity of chemical reactions and phase transitions.

Thermodynamics of open systems offers a new concept for the description of material objects, which are far from equilibrium, so that all real processes like viscous flows, phase transition and chemical reactions are included [8,14]. The II. Law of Thermodynamics can be interpreted as an evolution law of all material systems, which are in interaction with their surroundings. Entropy provides additional information about processes inside systems. The convexity of the entropy informs us about the stability of the system states [11]. Under appropriate outer conditions the fluctuations can drive the systems towards instability. The consequence is the creation or the decay of dissipative structures. When new dissipative structures appear, the system is shifted further away from the thermodynamic equilibrium into a stable potential vortex. This transition is experimentally proved [3,4], numerically simulated [24] but not satisfactory explained.

The main idea of this new concept is based on the formulation of the condition of attenuation of fluctuations in the vicinity of the reference (or steady) state. It is essential to consider the existence of dissipative processes, in our case viscosity and thermal conductivity. The following Sect. 2 explains the theoretical basis, and Sect. 3 shows some consequences of the thermodynamic criterion for a solid body vortex and a free vortex. Both of these vortices play a decisive role in the operation of the vortex tube; therefore, precise experiments performed on this tube are used to compare with the conclusions of the mentioned theory. Section 4 explains then briefly the used numerical methods, before Sect. 5 shows several examples (vortex tube, Couette flow, swirling flow and tropical cyclone) for which thermodynamics stability criterion is validated by experiments and simulations. Finally the main conclusions are summarized.

2 Theoretical basis: thermodynamic conditions of stability

The stability of the swirl flow in a vortex tube is studied on the base of non-equilibrium thermodynamics. The fluid viscosity is represented by the dissipative part of the stress tensor $\mathbf{t}_{\mathrm{dis}}$ and the heat transfer by the heat flux $\mathbf{q}$. The II. Law of Thermodynamics, the so-called thermodynamic stability criterion, has the form

$$\pi = \rho \underbrace{\left[T\dot{s} - \dot{u} - p\dot{\overline{\left(\frac{1}{\rho}\right)}} \right]}_{=0\ldots\text{Gibbs entropy definition}} - \frac{q^k}{T}\frac{\partial T}{\partial x^k} + t^{ki}_{\mathrm{dis}}\frac{\partial v_i}{\partial x^k} \geq 0, \tag{1}$$

$$-\frac{\rho}{2}\dot{\overline{d^2 u}} = \pi \geq 0 \ \ldots \ \text{stability condition}$$

which is known as the *fundamental thermodynamic (Clausius-Duhem) inequality* [11,14]. This inequality gives both the Gibbs definition of entropy by internal energy $u = u(s, \rho)$ and the Gibbs thermodynamic stability condition $d^2u \geq 0$ [16]. The Gibbs stability condition is a consequence of the inequality $\dot{\overline{d^2u}} \leq 0$, which is taken as the material derivative of the Lyapunov function of the Gibbs stability condition $d^2u \geq 0$. The stable thermodynamic systems have to obey both, i.e. the condition $d^2u \geq 0$ (-stability of the state) and $\dot{\overline{d^2u}} \leq 0$ (-stability of the process) [11]. The fact that thermodynamic arguments lead to finding a suitable form of the Lyapunov function, which ensures the stability of the velocity field described by the Navier–Stokes equations, is shown, for example, in [7].

The fundamental thermodynamic inequality (1) was formulated by the II. Law of Thermodynamics using the internal energy. However, for the processes with dominant convection is more convenient the specific total enthalpy [19–23,27]

$$h_\mathrm{t} = u + \frac{p}{\rho} + \frac{v^2}{2} + \phi = h(T, p) + \frac{v^2}{2} + \phi, \tag{2}$$

Here we introduce the additional energy ϕ, which is induced by the gravity or due to the non-inertial motion of the system as a whole. An important case is, for example, the movement of the Earth's atmosphere, where the Coriolis acceleration takes a dominant role [10,20]. For our purpose, it is convenient to formulate the I. Law of Thermodynamics in terms of total enthalpy

$$\rho\dot{h}_\mathrm{t} - \frac{\partial p}{\partial t} = -\frac{q^k}{T}\frac{\partial T}{\partial x^k} + \frac{\partial\left(t^{ki}_\mathrm{dis}v_i\right)}{\partial x^k} \tag{3}$$

and the fundamental thermodynamic inequality (1) has the alternative form

$$\begin{gathered}\tilde{\pi} = \rho\underbrace{\left(T\dot{s} - \dot{h}_\mathrm{t} + \frac{1}{\rho}\frac{\partial p}{\partial t}\right)}_{=0\ \ldots\ \text{entropy definition}} - \frac{q^k}{T}\frac{\partial T}{\partial x^k} + \frac{\partial\left(t^{ki}_\mathrm{dis}v_i\right)}{\partial x^k} \geq 0, \\ -\frac{\rho}{2}\dot{\overline{d^2h_\mathrm{t}}} = \tilde{\pi} \geq 0 \ \ldots\ \text{stability condition for processes with convection}\end{gathered} \tag{4}$$

The specific total enthalpy is a function of the entropy and the pressure, i.e. $h_\mathrm{t} = h_\mathrm{t}(s, p)$, and satisfies the general relation

$$\dot{h}_\mathrm{t} = T\dot{s} + \frac{1}{\rho}\frac{\partial p}{\partial t}. \tag{5}$$

For the case without convection, it turns into the classical Gibbs definition in Eq. (1) using enthalpy. The fundamental thermodynamic inequality has the form $\tilde{\pi} \geq 0$. All dissipative processes in the system, which is in thermodynamic equilibrium, which we will call a *reference state* (denoted by subscript "0"), are zero. Considering the rapid temporal change of fluctuations, this reference state changes only very slowly in time. Such a reference state, $h_{\mathrm{t}0} = h_\mathrm{t}(\mathrm{s}_0, \mathrm{p}_0)$, has a dissipation extremum, i.e. its material (convective) derivative is equal to zero

$$T_0\dot{s_0} - \dot{h}_{\mathrm{t}0} + \frac{1}{\rho_0}\frac{\partial p_0}{\partial t} = 0, \quad \tilde{\pi} = \tilde{\pi}_0 = 0 \tag{6}$$

Now, let us suppose that the system deviates ($s = s_0 + \delta s,\ p = p_0 + \delta p$) from this reference state and its total enthalpy changes. The deviations (fluctuations) $\delta s,\ \delta p$ generate a dissipation $\tilde{\pi} \geq 0$, i.e.

$$T_0\dot{s} - \dot{h}_\mathrm{t} + \frac{1}{\rho_0}\frac{\partial p}{\partial t} = \tilde{\pi}_0 + \tilde{\pi} = \tilde{\pi} \geq 0 \tag{7}$$

Expanding the total enthalpy around the reference state (6) and inserting this into the dissipation inequality (7) gives

$$
\begin{aligned}
&h_{\mathrm{t}}(s,\,p) = h_{\mathrm{t}0} + dh_{\mathrm{t}0} + \frac{1}{2}d^2h_{\mathrm{t}0} + \cdots\,,\\
&-\dot{\overline{dh_{\mathrm{t}0}}} + T_0\dot{\overline{\delta s}} + \frac{1}{\rho_0}\frac{\partial \delta p}{\partial t} = \tilde{\pi}_0 = 0 \quad \text{extremum condition for } \tilde{\pi}\\
&-\frac{1}{2}\dot{\overline{d^2h_{\mathrm{t}0}}} = \tilde{\pi} = \frac{q^k}{T}\frac{\partial T}{\partial x^k} + \frac{\partial (t^{ki}_{\mathrm{dis}}v_i)}{\partial x^k} \geq 0 \quad \text{stability condition}
\end{aligned}
\tag{8}
$$

This inequality is an alternative form of the *thermodynamic condition of stability for processes with convection* (4). The dissipation $\tilde{\pi}$ is the second-order term in the total enthalpy change. The derivation is similar to the derivation of the classical Gibbs stability conditions (1). Thermodynamic fluid systems with dominant convection are stable when the inequalities both for the second differential $d^2h_{\mathrm{t}} \geq 0$ and for its material derivative $\dot{\overline{d^2h_{\mathrm{t}}}} \leq 0$ are satisfied. $d^2h_{\mathrm{t}} \geq 0$ is the Lyapunov function of stability [11]. If the inequality (4) is violated, convective instability can occur [19–21,23,25].

The fundamental importance of the specific total enthalpy for continuum mechanics was first shown by Seliger, and Whitham, who formulated Hamilton's principle of the least action [27]. After standard analysis (adoption $\mathbf{grad}h_{\mathrm{t}}$ in the energy equation), and after reorganization of some terms, we obtain the alternative form of *the momentum equation*. This equation, which combines the classical balance of momentum (balance of forces) and the balance of internal energy, is known as the *Crocco equation* (9). This equation is limited to the *steady case only* [2]. The important role of the $\mathbf{grad}h_{\mathrm{t}}$, $\mathbf{grad}s$ and the friction forces for the vorticity generation is evident

$$
(\mathbf{v}\times\mathbf{rot}\,\mathbf{v})_i = \frac{\partial h_{\mathrm{t}}}{\partial x^i} - T\frac{\partial s}{\partial x^i} - \frac{\partial t^{li}_{\mathrm{dis}}}{\rho\partial x^l} \quad \text{Crocco's theorem} \tag{9}
$$

The friction (dissipative) forces in an actual system are established explicitly by the dissipative part of the stress tensor $\mathbf{t}_{\mathrm{dis}}$. Nevertheless, even within flows of a constant total enthalpy, i.e. $\dot{h}_{\mathrm{t}} = 0$, the *entropy gradient can induce vortex generation*. This is the case with an additional heat release, e.g. by condensation $T(\partial s/\partial x^i) = h_{\mathrm{vl}}(\partial(w_{\mathrm{v}}/\partial x^i)$. Here $h_{\mathrm{vl}} > 0$, $[\mathrm{Jkg}^{-1}]$ is the heat of evaporation and w_{v} is the mass concentration of the vapour. The vortex magnitude can be substantially affected by this process.

For the simplified flow, $v_\varphi = v_\varphi(r)$, $T = T(r)$ *the thermodynamic condition for the stability of the process* (8) has the form

$$
\tilde{\pi} = \frac{\lambda}{T}\left(\frac{\partial T}{\partial r}\right)^2 + \mu_{\mathrm{mol}}\left[\left(\frac{\partial v_\varphi}{\partial r}\right)^2 + v_\varphi\frac{\partial^2 v_\varphi}{\partial r^2} - \frac{v_\varphi}{r}\frac{\partial v_\varphi}{\partial r}\right] + \frac{\partial \mu_{\mathrm{mol}}}{\partial r}\left(v_\varphi\frac{\partial v_\varphi}{\partial r} - \frac{v_\varphi^2}{r}\right) \geq 0 \tag{10}
$$

Considering that the thermal conductivity is a positive coefficient $\lambda > 0$, the associated term is always positive and will only have a stabilizing effect. We therefore focus only on the influence of the flow field $v_\varphi(r)$, where the molecular viscosity μ_{mol} plays a dominant role. The following approximation can be applied as the flow model in a vortex tube

$$
v_\varphi = \omega r \quad \text{then} \quad \tilde{\pi} = 0 \quad \text{solid body vortex} \tag{11}
$$

$$
v_\varphi = \Gamma/r \quad \text{then} \quad \tilde{\pi} = 4\mu_{\mathrm{mol}}\frac{\Gamma^2}{r^4} - \frac{2\Gamma^2}{r^3}\frac{\partial \mu_{\mathrm{mol}}}{\partial r} \geq 0 \quad \text{potential vortex} \tag{12}
$$

It follows that the solid body vortex is on the onset of stability and the potential vortex is stable for constant molecular viscosity μ_{mol}. This conclusion is also a consequence of viscosity-induced dissipation ($t^{ki}_{\mathrm{dis}}\frac{\partial v_i}{\partial x^k} \geq 0$, see (1)). This dissipation is zero for a solid body vortex and nonzero and positive for a potential vortex.

3 Consequences of thermodynamic stability conditions

The change of the specific total enthalpy (2) for a non-equilibrium state is given by equation (5). From the second differential of the specific total enthalpy depending on the variables T, p we obtain by the same procedure, which has obtained the classical Gibbs condition of thermodynamic stability $d^2u \geq 0$ [11,14,16], the stability condition for processes with convection. The result is *the thermodynamic stability condition of the reference state* (6) in the form

$$\frac{1}{2}d^2h_\mathrm{t} = \frac{1}{2}\left[\frac{c_\mathrm{p}}{T}(\delta T)^2 - \frac{1}{\rho^2 c^2}(\delta p)^2\right] > 0$$
$$\text{for} \quad c_\mathrm{p} = T\left(\frac{\partial s}{\partial T}\right)_\mathrm{p}, \quad c^2 = \left(\frac{\partial p}{\partial \rho}\right)_\mathrm{s} \tag{13}$$

This inequality indicates the destabilizing effect of pressure pulsations ($\delta p \neq 0$). This effect is generally very significant and leads to flow instabilities. In some special cases, however, which are practically very significant, a correlation can be found between pressure and temperature fluctuations such that the inequality (13) can be satisfied. The destabilizing term can be neglected, e.g. for incompressible fluids with high viscosity. From a practical point of view, a very important case is a flow in which the total enthalpy of the corresponding material point, which is moving with the velocity v_φ, is conserved, i.e. $h_\mathrm{t}(T, p) = const$. This situation occurs for steady isentropic flow (5). In this case, the condition is redundant and does not give any additional information.

We will theoretically analyse the flow and temperature fields in the vortex tube while neglecting the effect of viscosity on the inner walls of the tube. Assume $h_\mathrm{t}(T, p, v_\varphi) = const$, see (2) in the region $r \in (R_1, R_2)$, where $v_{\varphi 1} = v_\varphi(R_1)$, $v_{\varphi 2} = v_\varphi(R_2)$ holds at the boundaries of the region. In the case of a purely rotational flow, the independent variables are

$$v_\mathrm{r},\ v_\mathrm{z} \ll v_\varphi = v_\varphi(r),\ T = T(r),\ p = p(r),\ \phi = 0. \tag{14}$$

Then, the temperature and pressure depend on the velocity v_φ.

The material derivative of the specific total enthalpy depends on the radial coordinate r only, i.e.

$$v_\mathrm{r}\frac{\partial h_\mathrm{t}}{\partial r} + v_\varphi\frac{\partial h_\mathrm{t}}{r\partial \varphi} + v_\mathrm{z}\frac{\partial h_\mathrm{t}}{\partial z} = v_\mathrm{r}\frac{\mathrm{d}h_\mathrm{t}}{\mathrm{d}r}$$
$$= v_\mathrm{r}\left[\frac{1}{2}\frac{\mathrm{d}v_\varphi^2}{\mathrm{d}r} + \left(\frac{\partial h}{\partial T}\right)_\mathrm{p}\frac{\mathrm{d}T}{\mathrm{d}r} + \left(\frac{\partial h}{\partial p}\right)_\mathrm{T}\frac{\mathrm{d}p}{\mathrm{d}r}\right] = 0 \tag{15}$$

One of the prerequisites for fulfilling this equation is:

$$v_\mathrm{r} \neq 0 \quad \text{and} \quad \mathrm{d}h_\mathrm{t}/\mathrm{d}r = 0 \tag{16}$$

The condition (15) defines the *steady state* of the corresponding reference state (6). The thermodynamic derivatives in the steady-state condition (15) are

$$\left(\frac{\partial h}{\partial T}\right)_\mathrm{p} = c_\mathrm{p}, \quad \left(\frac{\partial h}{\partial p}\right)_\mathrm{T} = \frac{1}{\rho} - T\left(\frac{\partial(1/\rho)}{\partial T}\right)_\mathrm{p} \tag{17}$$

so that the condition (15) has the form

$$\frac{\mathrm{d}h_\mathrm{t}}{\mathrm{d}r} = \frac{1}{2}\frac{\mathrm{d}v_\varphi^2}{\mathrm{d}r} + \frac{1}{\rho}\frac{\mathrm{d}p}{\mathrm{d}r} + c_\mathrm{p}\frac{\mathrm{d}T}{\mathrm{d}r} - T\left(\frac{\partial(1/\rho)}{\partial T}\right)_\mathrm{p}\frac{\mathrm{d}p}{\mathrm{d}r} = 0. \tag{18}$$

For an incompressible flow, the last term is equal to zero. However, the fluid compressibility plays a decisive role for the vortex tube performance.

For an ideal gas $p = \rho RT$, the enthalpy does not depend on the pressure $(\partial h/\partial p)_\mathrm{T} = 0$. However, for all real gases the enthalpy slightly depends on pressure. Therefore, this term is very important for the derivation of the stability condition. The *distinction between incompressible and compressible flows* gives new insight

into the rotational flow stability. The pressure gradient for the rotational field (14) follows from the balance of momentum

$$\frac{v_\varphi^2}{r} = \frac{1}{\rho}\frac{\mathrm{d}p}{\mathrm{d}r} \tag{19}$$

Inserting this condition into Eq. (15) $T\ (\partial(1/\rho)/\partial T)_\mathrm{p} = 1/\rho$, the actual form of the steady-state conditions (16) is

$$\begin{gathered}\frac{\mathrm{d}h_\mathrm{t}}{\mathrm{d}r} = \frac{1}{2}\frac{\mathrm{d}v_\varphi^2}{\mathrm{d}r} + \frac{v_\varphi^2}{r} + c_\mathrm{p}\frac{\mathrm{d}T}{\mathrm{d}r} - \frac{1}{\rho}\frac{\mathrm{d}p}{\mathrm{d}r} = \\ \underbrace{\frac{\mathrm{d}(rv_\varphi)^2}{2r^2\mathrm{d}r}}_{\text{mechanical stability}} + \underbrace{c_\mathrm{p}\frac{\mathrm{d}T}{\mathrm{d}r} - \frac{v_\varphi^2}{r}}_{\text{thermal stability}} = 0\end{gathered} \tag{20}$$

This equation defines the steady state (15), which is stable, if the condition of the total enthalpy minimum (13) is fulfilled. Therefore, in order to achieve a steady state, the criterion of mechanical stability must be mutually compensated with the criterion of thermal stability

$$\underbrace{\frac{\mathrm{d}(rv_\varphi)^2}{2r^2\mathrm{d}r}}_{\text{Rayleigh criterion}} = \underbrace{-c_\mathrm{p}\frac{\mathrm{d}T}{\mathrm{d}r} + \frac{v_\varphi^2}{r}}_{\text{Thermal criterion}} \tag{21}$$

The fluid flow is stable when if inequalities are satisfied simultaneously. However, it is not valid in general and the Rayleigh criterion is in contradiction with the thermodynamic stability criterion, according to which the solid body vortex is on the onset of stability (11). The evolution of the vortex structure in a vortex tube is discussed in Sect. 5.1. The solid body vortex transforms to a potential vortex, as demonstrated in the following.

3.1 Solid body vortex

The flow field of a solid body vortex is defined as

$$\mathbf{v} = (v_\varphi, v_\mathrm{z}, v_\mathrm{r}),\ v_\varphi = \omega r,\ v_\mathrm{z} = 0,\ v_\mathrm{r} = 0,\ T = T(r),\ p = p(r),\ \phi = 0 \tag{22}$$

where ω is the constant angular velocity. The mechanical stability condition results in

$$\frac{\mathrm{d}(rv_\varphi)^2}{2r^2\mathrm{d}r} = 2\omega^2 r > 0 \tag{23}$$

and is satisfied for all ω. After integration (for $c_\mathrm{p} = const.$) the corresponding thermally criterion (21) gives

$$c_\mathrm{p}(T_2 - T_1) \le \frac{v_{\varphi 2}^2}{2} - \frac{v_{\varphi 1}^2}{2} = \omega^2(R_2^2 - R_1^2). \tag{24}$$

Accordingly, the temperature T_1 at the inner radius R_1 of the tube must be lower than the temperature T_2 at the outer radius R_2. The inner and outer radii $R_1,\ R_2$, respectively, are only hypothetical, with $R_1 \to 0$ and $R_2 \to D_0/2$, see Sect. 5.1, where the experiments within a vortex tube are presented. Although the criterions of mechanical stability and thermal stability are both met, the thermodynamic criterion indicates a state at the onset of stability (-marginal stability (11)).

The steady-state condition, see Eq. (15), can be satisfied even for the total enthalpy depending on the coordinate r

$$v_\mathrm{r} = 0 \quad \text{and} \quad \frac{\mathrm{d}h_\mathrm{t}}{\mathrm{d}r} \neq 0. \tag{25}$$

This assumption is fulfilled at the fluid entrance of the tube. By using the Crocco theorem (9) for the simplified flow (22) we have

$$T\frac{\partial s}{\partial r}+(\mathbf{v}\times\mathbf{rot}\,\mathbf{v})_{\mathrm{r}}=\frac{\partial h_{\mathrm{t}}}{\partial r}-\frac{\partial t_{\mathrm{dis}}^{lr}}{\rho\partial x^{l}}$$
$$T\frac{\partial s}{\partial r}+\frac{v_{\varphi}}{r}\frac{\partial(rv_{\varphi})}{\partial r}=T\frac{\partial s}{\partial r}+2r\omega^{2}=\frac{\partial h_{\mathrm{t}}}{\partial r} \tag{26}$$

where the vorticity in cylindrical coordinates $(\varphi,\ z,\ r)$ is given by

$$\mathbf{rot}\,\mathbf{v}=\left(\frac{\partial v_{\mathrm{z}}}{r\partial\varphi}-\frac{\partial v_{\varphi}}{\partial z},\frac{\partial v_{\mathrm{r}}}{\partial z}-\frac{\partial v_{\mathrm{z}}}{\partial r},\frac{1}{r}\frac{\partial(rv_{\varphi})}{\partial r}-\frac{\partial v_{\mathrm{r}}}{r\partial\varphi}\right) \tag{27}$$

According to assumption (14), we neglect the effect of molecular viscosity on the inner wall of the pipe, so the dissipative part t_{dis}^{lr} of the stress tensor has no effect on the change in rotation of the inlet vortex and does not contribute to the radial velocity v_{r}. For an isentropic flow this equation gives after integration a basic relation for the vortex tube with the solid body approximation

$$\Delta h_{\mathrm{t}}=h_{\mathrm{t}}(r)-h_{t1}=2\omega^{2}\int_{R_1}^{r}r\mathrm{d}r=\omega^{2}\left(r^{2}-R_1^{2}\right)=v_{\varphi}^{2}-v_{\varphi_1}^{2} \tag{28}$$

The parabolic growth of the total enthalpy is confirmed both by experiments and numerical simulations. The temperature difference between the vortex core, radius R_1 and the outer region is given by

$$h_{\mathrm{t}}(r)-h_{\mathrm{t}1}=c_{\mathrm{p}}T+\frac{v_{\varphi}^{2}}{2}-c_{\mathrm{p}}T_1-\frac{v_{\varphi_1}^{2}}{2}=v_{\varphi}^{2}-v_{\varphi_1}^{2}$$
$$T-T_1=\frac{v_{\varphi}^{2}-v_{\varphi_1}^{2}}{2c_{\mathrm{p}}} \tag{29}$$

compared with the inequality (24). The formula (29) gives the maximum temperature difference, which can be reached close to the inlet. For instance, the maximum velocity at the tube inner wall (radius R_2) is $v_{\varphi}=166\,[\mathrm{ms}^{-1}]$ for $\omega=6670\,[\mathrm{s}^{-1}]$ and for dry air with $c_{\mathrm{p}}\doteq 1000\,\mathrm{Jkg}^{-1}\mathrm{K}^{-1}$, Eq. (29) gives a limiting temperature difference of 13.8 K. For the actual velocity $v_{\varphi}=115\,[\mathrm{ms}^{-1}]$ the temperature difference is 6.6 K. A comparison with the experiment is shown in Sect. 5.1.

3.2 Potential vortex

In this case, the flow field is defined by

$$\mathbf{v}=(v_{\varphi},v_{\mathrm{z}},v_{\mathrm{r}}),\ v_{\varphi}=\frac{\Gamma}{r},\ v_{\mathrm{z}}=0,\ v_{\mathrm{r}}=0,\ T=T(r),\ p=p(r),$$
$$\text{where}\quad 2\pi\Gamma=\int_{0}^{2\pi}v_{\varphi}(r)rd\varphi \tag{30}$$

Here $2\pi\Gamma$ is the constant circulation of the velocity field of the corresponding vortex. From the Rayleigh criterion (21), one obtains

$$\frac{\mathrm{d}(rv_{\varphi})^{2}}{2r^{2}\mathrm{d}r}=0 \tag{31}$$

and then the thermal criterion (21) has the form

$$c_{\mathrm{p}}(T_2-T_1)=\frac{v_{\varphi_1}^{2}}{2}-\frac{v_{\varphi_2}^{2}}{2}=\frac{\Gamma^{2}}{2R_2^{2}}\left(\frac{R_2^{2}}{R_1^{2}}-1\right) \tag{32}$$

The inner radius of the vortex (core of the vortex) will in Eq. (30) be denoted by R_1 and the outer radius by R_2. Due to the velocity distribution (30) with $v_{\varphi_1}>v_{\varphi_2}$, the temperature in the core of the vortex has to be lower

than the temperature close to the outer wall. As a consequence *both conditions of the steady-state stability* (15) *are satisfied*. In addition, the potential vortex is also stable according to the thermodynamic stability criterion of the process (12). The balance of momentum (Crocco's theorem) (9) for the simplified flow (30) reads

$$(\mathbf{v} \times \mathbf{rot}\ \mathbf{v})_\mathrm{r} = 0 = \frac{\partial h_\mathrm{t}}{\partial r} - T\frac{\partial s}{\partial r} \tag{33}$$

For an isentropic flow, this equation is satisfied for constant enthalpy, i.e. $h_\mathrm{t}(r) = const$. Hence,

$$c_\mathrm{p} T_1 + \frac{\Gamma^2}{2r_1^2} = c_\mathrm{p} T + \frac{\Gamma^2}{2r^2} \tag{34}$$

which has the same form as condition (32)

$$T - T_1 = \frac{\Gamma^2}{2c_\mathrm{p}} \left(\frac{1}{r_1^2} - \frac{1}{r^2} \right) \Bigg|_{\mathrm{r}\to\infty} = \frac{v_{\varphi_1}^2}{2c_\mathrm{p}} \tag{35}$$

This equation is identical with the classical isentropic concept, see (5) for $\partial p/\partial t = 0$.

4 Applied numerical methods

Numerical simulations provide additional details about the physics and stability in a vortex tube. In a previous work, the swirl tube was simulated via detached Eddy simulations (DES) using the open-source code OpenFOAM and validated by experimental data [4]. The Spalart-Allmaras turbulence model [26] was used, which solves the near-wall region with the RANS (Reynolds-averaged Navier–Stokes) equations and the free stream region via LES (Large Eddy Simulation). Numerical simulations of the flow in a vortex tube give additional insight into the distribution of all measurable parameters, see Sect. 5.1. The dissipation, that is not directly measurable, is defined as

$$\epsilon = \nu \overline{\frac{\partial u_i}{\partial x_j} \frac{\partial u_i}{\partial x_j}} \tag{36}$$

Here ν is the kinematic viscosity and u_i is the velocity fluctuation. The size of the dissipation is partly influenced by the used calculation algorithm and the size of the used calculation mesh. From the good agreement between numerical results with experiments, it follows that the dissipation corresponds to reality. A detailed description is given in [24].

5 Experiments and comparison with numerical simulation

Flow properties in vortex tubes have been studied both theoretically and experimentally since their invention [13]. A specific use is the energy separation, which is a consequence of the specific properties of the swirl flow. To determine the basic properties of this flow, two types of experiments were proposed: a vortex in a cylindrical tube—(*vortex tube*) and a vortex in free space—(*swirl flow*).

Two kinds of independent experiments were performed to prove the transformation of an annular swirl flow into a potential vortex flow. Experiments based in a vortex tube were carried out at the Institute of Aerospace Thermodynamics in Stuttgart, and experiments in an annular nozzle were performed at the Institute of Thermomechanics CAS in Prague.

5.1 Vortex tube experiments

The vortex tube measurements have been taken at the experimental apparatus at the Institute of Aerospace Thermodynamics in Stuttgart shown in Fig. 1. Flow field measurements via PIV (particle image velocimetry) have been taken as well as heat transfer measurements using the well-established transient thermochromic liquid crystal (TLC) technique. The flow through the apparatus is sucked by a vacuum pump, and the mass flow is measured with a laminar flow element (1) [3].

The flow is then seeded with oil particles for the PIV measurements or heated in a mesh heater (3) for the TLC experiments. Next, the air enters tangentially into the swirl tube (5) and exits into an outlet plenum, which is connected to the vacuum pump. The dimensions and the used coordinate system are shown in Fig. 2. The tube represents an upscaled generic model of a turbine blade leading edge swirl chamber. The tube has an inner diameter of $D_0 = 50$ mm and a length of $L/D_0 = 20$. The swirl is induced through two tangential injections. The first experimental values showing the local distribution of velocity and temperature performed using the PIV method and the thermochromic crystal technique are shown in Fig. 3.

Flow parameters of the experiments are defined by the inflow Reynolds number Re_{z0}, which is based on the tube inlet diameter $D_0 = 2R_0$ and the corresponding incoming mass flow rate $\dot{m}$, therefore

$$Re_z = \frac{4\dot{m}}{\pi D_0 \mu} \tag{37}$$

Moreover, the fluid rotation is defined by the dimensionless swirl number

$$S = \frac{2\pi \int_0^{R_0} \rho v_\varphi v_z r^2 \mathrm{d}r}{2\pi R_0 \int_0^{R_0} \rho v_z^2 r \mathrm{d}r} \tag{38}$$

Since the velocity profiles are not known in advance, a geometric swirl number [24] is introduced

$$S_{\mathrm{geo}} = \frac{\pi R_0^2 (R_0 - h/2)}{2 R_0 w h} \tag{39}$$

where the parameters h and w represent the height and the width of the tangential inlet, respectively, see Fig. 2.

The velocity profile in the pipe has been measured by using PIV. Results are shown in Fig. 3 [3] for four axial positions z/D_0. The profile is characterized as a solid body vortex in the inlet region and as a potential vortex near the outlet [23]. This is schematically illustrated in Fig. 3a. The temperature distribution along the tube is depicted in Fig. 3c

With the assumption of a homentropic flow (uniform entropy s) the radial enthalpy is evaluated based on the velocities using Crocco's theorem (9), as follows $\partial h_c/\partial r = (\mathbf{v} \times \mathbf{rot}\ \mathbf{v})_r$ and is shown in Fig. 4c. A parabolic growth of the total enthalpy near the inlet is apparent, and the magnitude decreases towards the tube outlet.

Figure 4 shows numerical prediction by using the compressible delayed detached Eddy simulations (DDES). All numerical simulations were conducted with a no-slip condition at the wall (v_w=0) and an isothermal wall

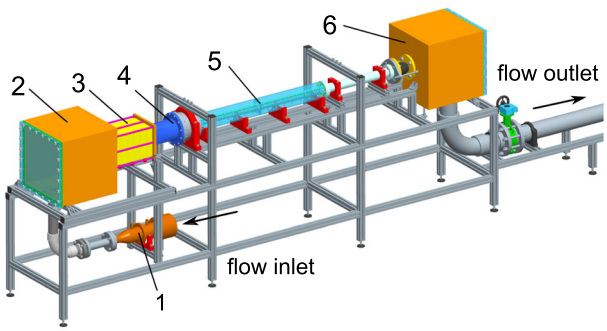

Fig. 1 Experimental apparatus (CAD) with (1) laminar flow element, (2) inlet plenum, (3) mesh heater, (4) swirl generator, (5) swirl tube and (6) outlet plenum [3]

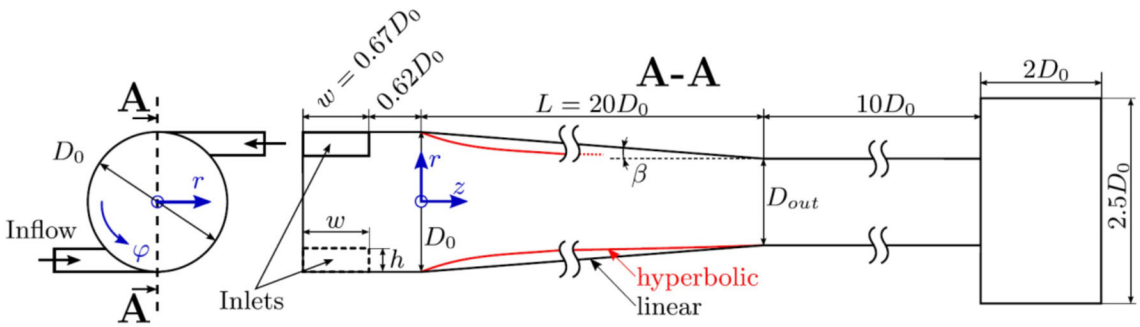

Fig. 2 Convergent swirl chamber [24]

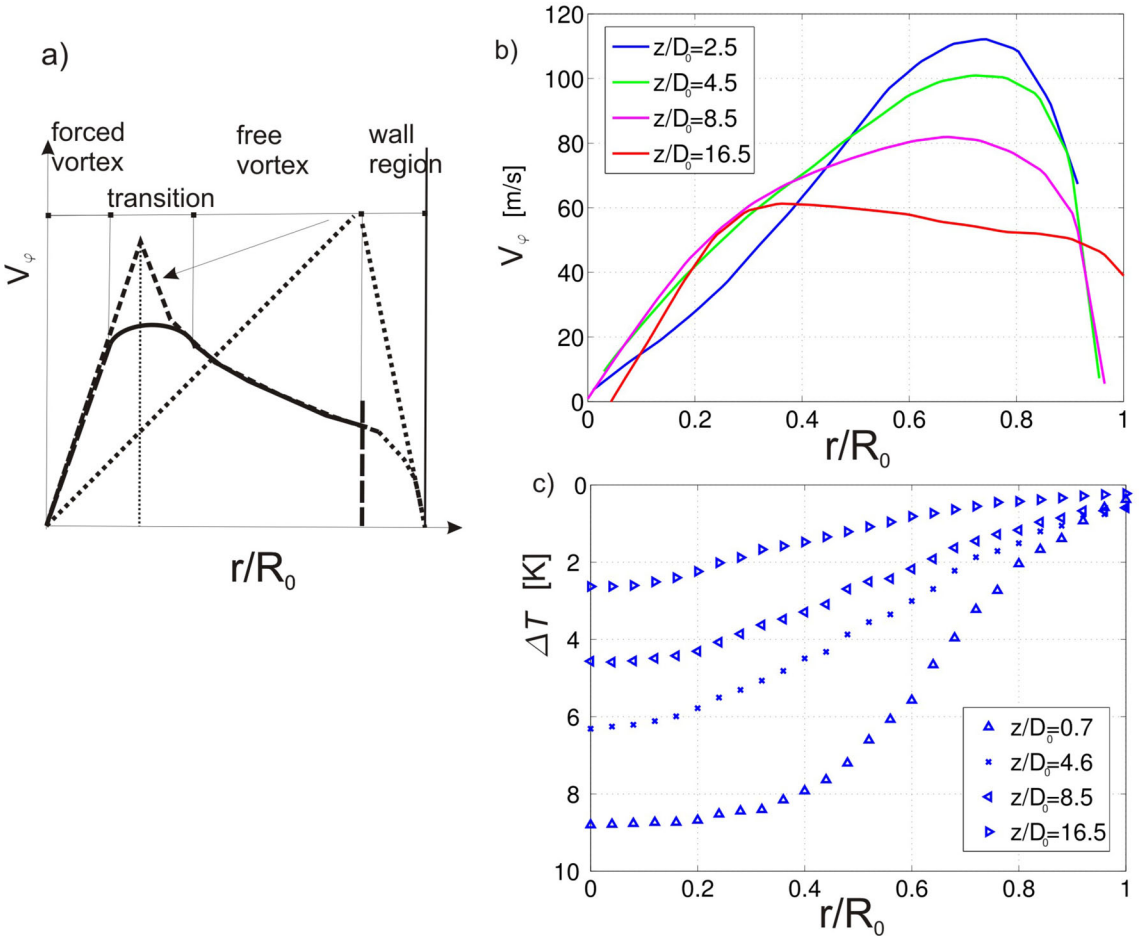

Fig. 3 **a** Rankine vortex formation. A forced vortex has the properties of a solid body vortex. A free vortex represents a potential vortex. **b** Tangential velocities distribution V_φ and temperature differences **c** in radial direction for different distances from the inlet. Tube diameter is constant $D_0 = 50$ mm, and $\mathrm{Re_z} = 40{,}000$ [3,24]

temperature ($T_\mathrm{w} = 293$ K). Consequently, the total enthalpy at the wall yields

$$h_{\mathrm{t,w}} = c_\mathrm{p} T_\mathrm{w} + \frac{\mathrm{v_w^2}}{2} = c_\mathrm{p} T_\mathrm{w} = 295.344 \, \frac{\mathrm{J}}{\mathrm{kg\,K}} \tag{40}$$

In Fig. 4 the radial coordinate r is scaled by the local tube radius $R(z)$ (see Fig. 2, Table 1), whereas the values of the velocity and the total enthalpy represent absolute quantities. The axial flow shows the maximum near

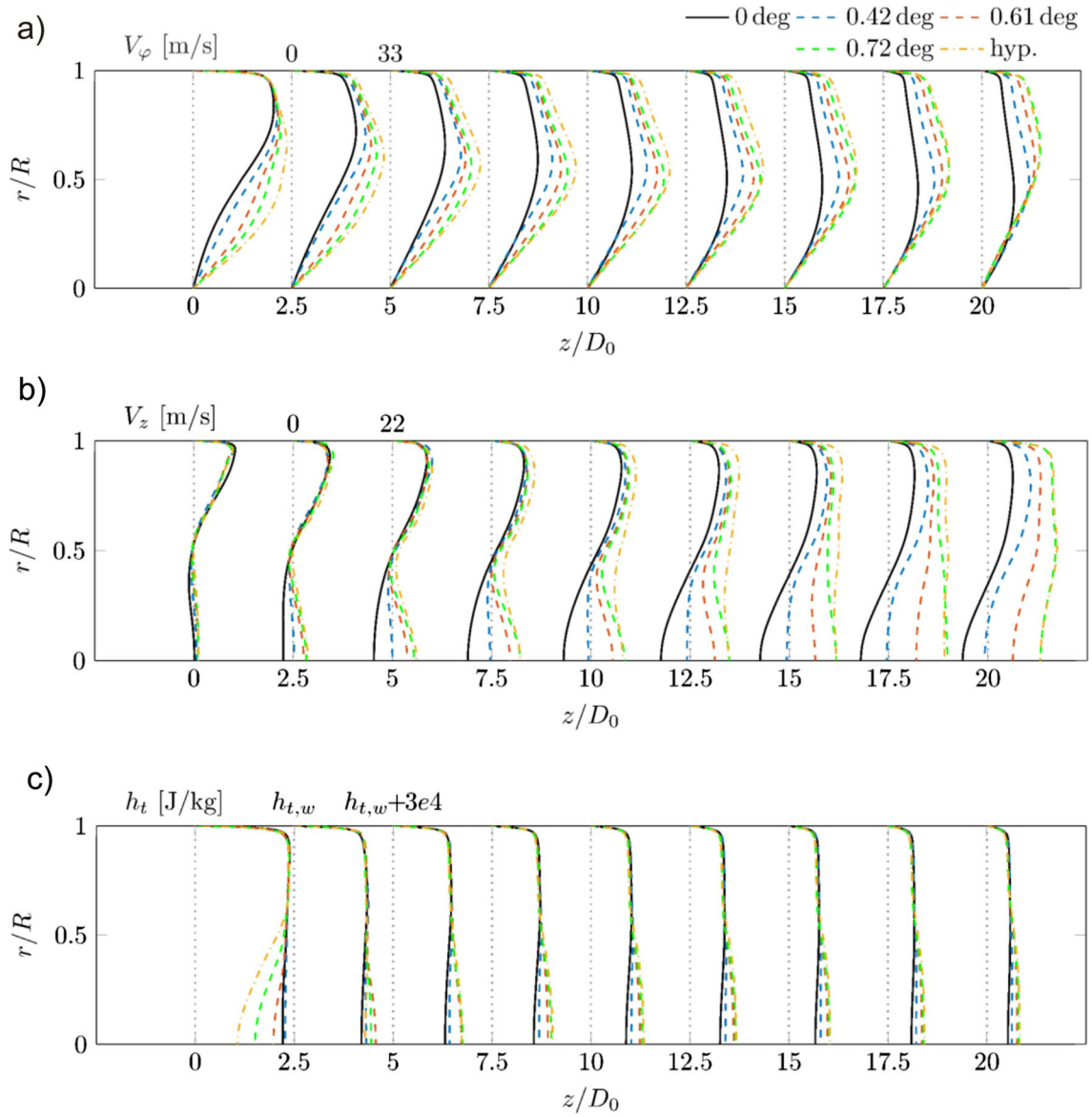

Fig. 4 Flow field in convergent swirl chambers Fig. 2 [24]. Absolute circumferential velocity V_φ, see **a** absolute axial velocity V_z, see **b** and parabolic growth of h_t (28) and its deviation from the total enthalpy h_{tw}, value (40), see **c**, respectively

the wall and a back flow region in the tube centre. This flow separation is caused by the Ranque–Hilsch effect, which creates a radial energy (temperature) separation in a vortex tube, see Fig. 3 [3].

The shown profiles represent compressible delayed detached Eddy simulations for an axial inflow Reynolds number Re_{z0} = 10,000 and a design swirl number S_{geo} = 5.3 for different geometries, according to Table 1. The transformation of the circumferential velocity v_φ from a solid body vortex, can be seen in Fig. 4a, and the equalization of the total enthalpy h_t is evident towards the end of the tube that is nicely visible in Fig. 4c.

5.2 Couette flow

To show the generality of the thermodynamic stability condition (8), the classical Couette flow between two cylinders [5] was investigated. Provided that the flow is isothermal and the fluid has a constant density and a constant viscosity, the exact solution of the Navier–Stokes equations for the flow field between two rotating cylinders was found to be a superposition of a solid body vortex and a potential vortex—(inviscid assumption).

Table 1 Investigated geometries

Geometry	D_0 (mm)	Area ratio A_{out}/A_0	Angle β	Diameter
1	50	1	0 deg	Linear
2	50	1/2	0.42 deg	Linear
3	50	1/3	0.61 deg	Linear
4	50	1/4	0.72 deg	Linear
5	50	1/4	Varying	Hyperbolic

The velocity field $v = (v_r, v_\varphi, v_z)$ and the pressure $p = p(r)$ depend for this case on the radius r

$$\begin{aligned} &v_r = v_z = 0 = v_\varphi = v_\varphi(r) = \omega(r)r \quad \text{for } \omega(r) = Ar + \frac{B}{r^2} \\ &A = -\Omega_1\eta^2\frac{1-\mu/\eta^2}{1-\eta^2},\ B = \Omega_1\frac{R_1^2(1-\mu)}{1-\eta^2} \quad \text{for } \mu = \Omega_2/\Omega_1,\ \eta = R_1/R_2 \end{aligned} \tag{41}$$

The radius of the outer cylinder is R_2 and its angular velocity is Ω_2 and for the inner cylinder is R_1, Ω_1, respectively. The non-dimensional quantities are $-\infty < \mu = \Omega_2/\Omega_1 < 1$, $0 < \eta = R_1/R_2 < 1$, $0 < \tilde{r} = r/R_2 < 1$. The Rayleigh criterion (21) gives

$$\begin{aligned} &\bar{\Omega}_R(\mu-\eta^2)[\eta^2(1-\mu)+\tilde{r}^2(\mu-\eta^2)] \geq 0, \\ &\text{where} \quad \bar{\Omega}_R = \frac{4\Omega_1^2}{\tilde{r}^2}(1-\eta^2)^2 > 0 \text{ and } 0 < \mu < 1, \\ &\text{then } \mu = \Omega_2/\Omega_1 > \eta^2 \quad \text{or} \quad \Omega_2 R_2^2 > \Omega_1 R_1^2 \quad \text{is a stability condition} \end{aligned} \tag{42}$$

According to this criterion, the Couette flow is stable if the angular momentum $\rho r v_\varphi$ increases in the $r-$direction. Considering that for a given ratio of R_1/R_2, which is always less than 1, the inner cylinder can rotate even faster than the outer one, see Fig. 5.

The thermodynamic stability criterion of the process (10), which respects the existence of viscosity, supplements the purely mechanical Rayleigh criterion with an additional condition that can be interpreted as the onset of coherent structures (Taylor–Couette flow). For the flow field specified by Eq. (41), we apply the simplified form (10) and we get

$$\frac{\tilde{\pi}}{\mu_{mol}} = \frac{4\Omega_1^2\eta^4(1-\mu)^2}{\tilde{r}^4(1-\eta^2)^2} \geq 0 \tag{43}$$

This inequality can also be interpreted in the following way

$$\begin{aligned} &\frac{\tilde{\pi}}{\mu_{mol}} = \frac{4\Omega_1^2\eta^4}{\tilde{r}^4} > 0 \\ &\text{for} \quad (1-\mu)^2 = (1-\eta^2)^2 \quad \text{-onset of coherent structures} \\ &\text{or } \Omega_1 = \Omega_2\left(\frac{R_1}{R_2}\right)^{-2} \text{ and } \Omega_1 = \Omega_2\left(2-\left(\frac{R_1}{R_2}\right)^2\right)^{-1} \end{aligned} \tag{44}$$

According to the thermodynamic criterion of stability of the process, the Taylor–Couette flow in this simplified formulation (41) is always stable. Only in the case of $\Omega_1 = \Omega_2$ it is at the limit of stability (solid body vortex (11) and coherent structures emerge. At high Reynolds numbers $\mathrm{Re} = \rho(R_2 - R_1)\Omega_1 R_1/\mu_{mol}$, the viscosity loses its stabilizing effect so coherent structures break up and laminar flow turns into turbulent flow. The limits of the onset of coherent structures are shown in Fig. 5.

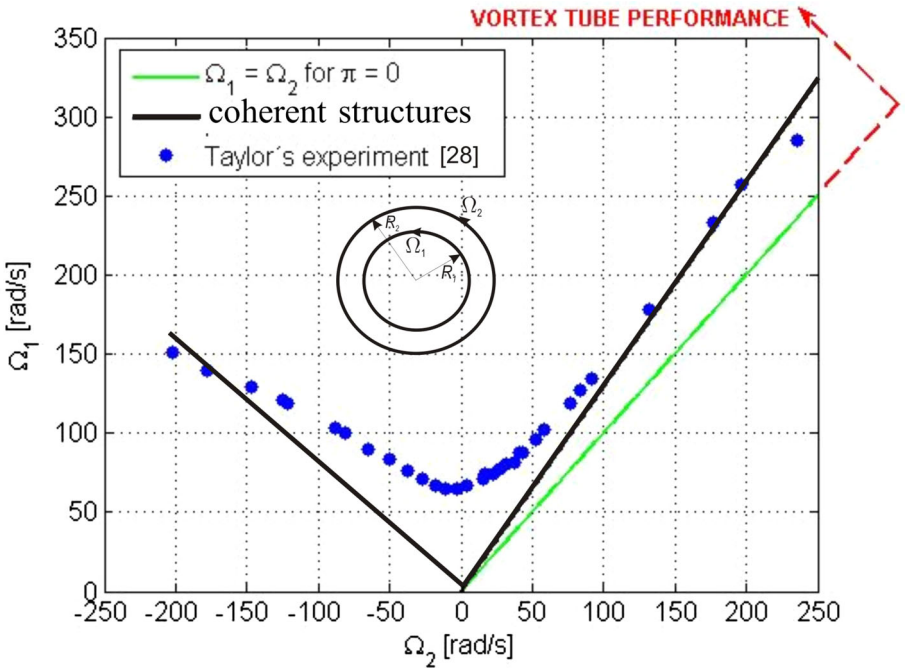

Fig. 5 Onset of coherent structures (instability) for a viscous flow between two rotating cylinders for $\eta = R_1/R_2 = 0.8798$ (Taylor–Couette flow) [28], see the sketch in Fig. The onset of instability is given by the black straight lines $\Omega_1 = 1.292\Omega_2$, for $\Omega_2 > 0$- (right) and for $-\Omega_2 \in (-250, 0)$ by $\Omega_1 = \frac{-\Omega_2}{\left(\frac{R_1}{R_2}\right)^2 - 2} = 0.815\Omega_2$-(left)

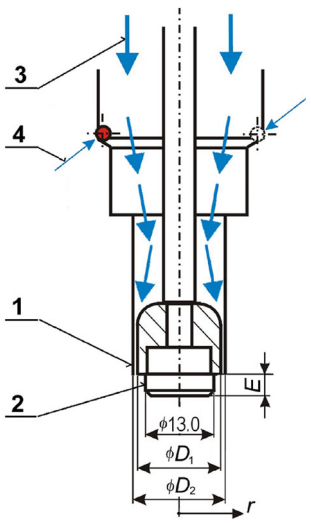

Fig. 6 The annular nozzle and tested configuration. 1: outer nozzle body, 2: nozzle centrebody, 3: axial air flow supply, 4: swirling air flow supply through a pair of tangential ports (diameter 3.1 mm); H: nozzle-to-wall spacing, E: centrebody extension. Dimensions: $D_2 = 17.6$ mm, $D_1 = 15.85$ mm, and $E = 4.1$ mm

5.3 Annular swirling jet experiments

The flow field of annular swirling jet was investigated experimentally with air as the working fluid [1]. The scheme of the present setup is shown in Fig. 6. The jets were issued from the annular nozzle with an outer and inner exit diameters of $D_2 = 17.60$mm and $D_1 = 15.85$ mm, respectively (i.e. the nozzle slot width is $b = (D_2 - D_1)/2 = 0.88$ mm and the diameter ratio is $D_1/D_2 = 0.90$).

The nozzle centrebody is extended at the outer nozzle lip by a distance of $E = 4.1\,\mathrm{mm}$. The settling chamber located upstream of the nozzle operated as the swirl generator. For this purpose, the chamber was supplied with axial (main) and swirling (tangential, control) air flow inlets with the mass fluxes $\dot{m}_z$ and $\dot{m}_\varphi$, respectively. Both fluxes were adjusted independently and were evaluated by the volumetric measurements by a pair of rotameters.

The Reynolds number is defined as $\mathrm{Re} = V D_2/\nu$, where V is the time average velocity at the nozzle exit, $V = (\dot{m}_z + \dot{m}_\varphi)/(\rho A)$ and A is the nozzle exit cross-sectional area, $A = \pi(D_2^2 - D_1^2)/4$. The Reynolds number based on the nozzle annular slot is defined as $\mathrm{Re_b} = Vb/\nu$.

The swirling strength of the flow is characterized by the swirl number S, similar to Eq. (38), and it is defined as the ratio of the axial flux of the angular momentum to the axial flux of the axial momentum multiplied by a characteristic radius

$$S = \frac{\displaystyle\int_{D_1/2}^{D_2/2} 2\pi\rho v_z v_\varphi r^2 \mathrm{d}r}{\dfrac{D_\mathrm{m}}{2}\displaystyle\int_{D_1/2}^{D_2/2} 2\pi\rho v_z^2 r \mathrm{d}r}. \tag{45}$$

Here v_z and v_φ are the axial and tangential velocity components at the nozzle exit, respectively, D_m is the mean diameter defined as $D_\mathrm{m} = (D_2 + D_1)/2$, and ρ is the air density and r is the diameter. In the present case with a narrow annular slot, the average axial and tangential velocity components at the nozzle exit cross section are assumed to be v_z and v_φ, respectively. Hence, the swirl number can be evaluated by $S \sim v_\varphi/v_z \tan(\varphi)$, where φ is the angle of yaw of the vector of the outlet velocity flow.

The experiment results in Fig. 7 show how the annular flow forms into a potential vortex. If the viscosity of the fluid is nonzero, the potential vortex is more stable under the given conditions than the solid body vortex, as can be seen from the thermodynamic stability condition (11) and (12).

5.4 Tropical cyclones—Rankine vortex approximation

Tropical cyclones can be approximated fairly well by a Rankine vortex [15]. The inner part (so-called eye) of the cyclone is modelled by a solid body vortex. In the following it is assumed that dry air of density ρ_a contains water in the form of vapour of density ρ_v. The mass concentration of the vapour is $w_\mathrm{v} = \rho_\mathrm{v}/\rho$. The total density of the moist air is equal to

$$\rho = \rho_\mathrm{a} + \rho_\mathrm{v} = \frac{M_\mathrm{a} p}{RT}\left[1 + \left(\frac{M_\mathrm{a}}{M_\mathrm{v}} - 1\right) w_\mathrm{v}\right]^{-1} \quad \text{for } p = p_\mathrm{a} + p_\mathrm{v} \tag{46}$$

The molecular mass of air and water are $M_\mathrm{a} = 0.02896\,\mathrm{kg\,mol^{-1}}$ and $M_\mathrm{v} = 0.018015\,\mathrm{kg\,mol^{-1}}$, respectively. The gas constant is $R = 8.314\,\mathrm{J\,mol^{-1}K^{-1}}$ and $c_{\mathrm{p\,a}} = 1006.5\,\mathrm{J\,kg^{-1}}$ is the specific heat at constant pressure of air. The concentration of water in the air in the form of water vapour is

$$w_\mathrm{v} = \frac{x}{1+x} = \frac{M_\mathrm{v}\phi p_\mathrm{sat}}{M_\mathrm{a} p - (M_\mathrm{a} - M_\mathrm{v})\phi p_\mathrm{sat}}, \quad x = \frac{\rho_\mathrm{v}}{\rho_\mathrm{a}},\ \phi = \frac{p_\mathrm{v}}{p_\mathrm{sat}} \tag{47}$$

where ϕ is the relative humidity, p_sat is the saturation pressure, and $x = w_\mathrm{v}/(1 - w_\mathrm{v}) \doteq w_\mathrm{v}$, for $w_\mathrm{v} \ll 1$ is the specific humidity (humidity ratio). The saturation pressure depends on the temperature only

$$p_\mathrm{sat} = 610.94 \exp\left[\frac{17.625(T - 273.15)}{T - 30.11}\right]\ [\mathrm{Pa}],\ T\ [\mathrm{K}] \tag{48}$$

For the description of atmospheric phenomena such as cyclones, which take place in the troposphere (from the surface of the earth to a maximum altitude of 18 km), the dependence of temperature, pressure and density on altitude z is important. Considering that the standard parameters at the Earth surface are $p_0 = 101.325\,\mathrm{kPa}$, $T_0 = 288.15\,\mathrm{K}$, $\rho_0 = 1.225\,\mathrm{kg\,m^{-3}}$ the following relations hold with sufficient accuracy

$$T(z) = T_0 - Lz\,[\mathrm{K}]$$
$$\text{for} \quad L = -\frac{\mathrm{d}T}{\mathrm{d}z} = 0.0065\,\mathrm{K\,m^{-1}} \text{ for moist air},\ L_\mathrm{d} = g/c_\mathrm{p} = 0.0098\,\mathrm{K\,m^{-1}} \text{ for dry air}$$

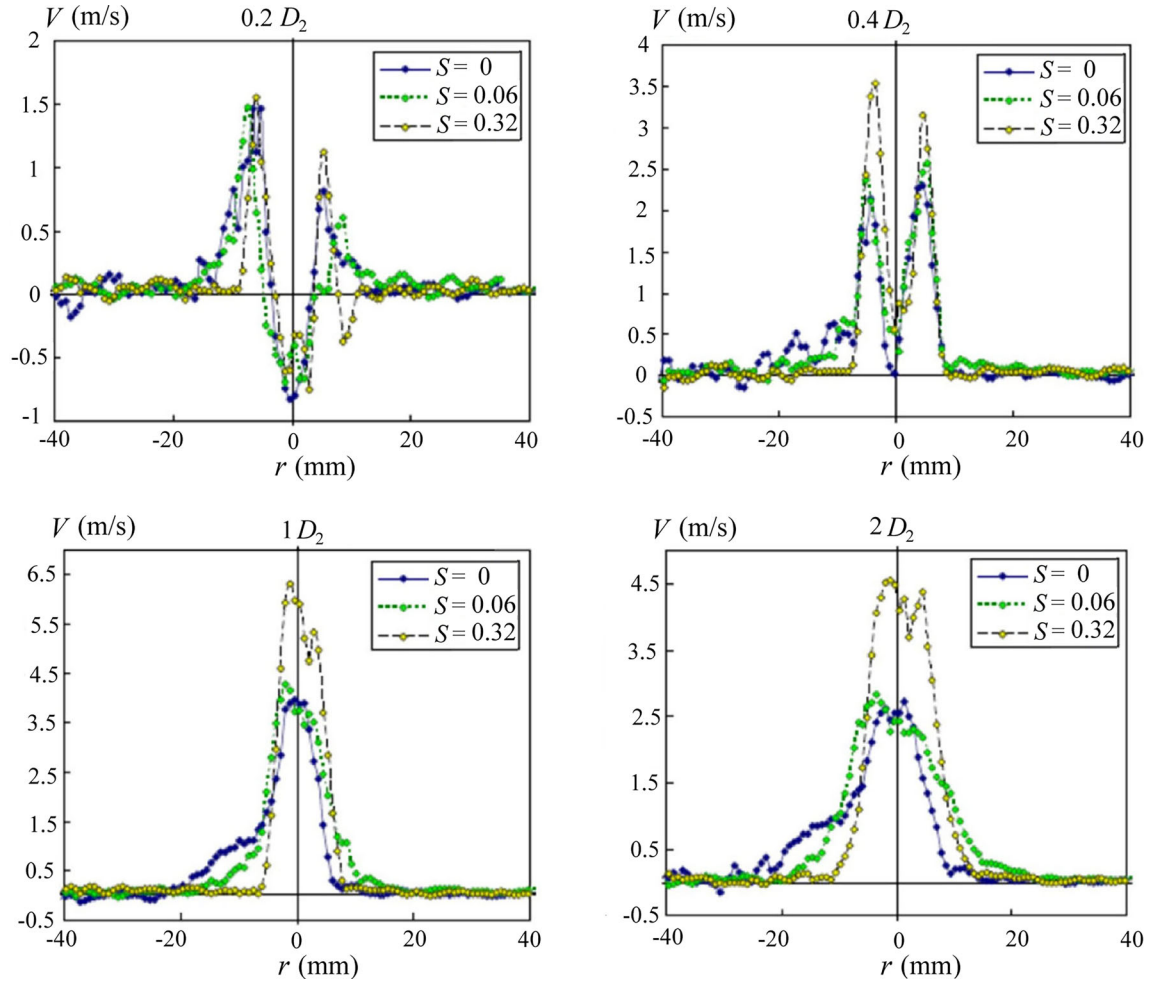

Fig. 7 PIV measurement with cross-stream velocity profiles and streamwise velocity component at different distances measured from the bottom part of the nozzle centrebody (0.2–2)D_2. The experiments were performed at Re = 5000 for five variants of the jets depending on the swirl number S from 0 to 0.32

$$\frac{\mathrm{d}p}{\mathrm{d}z} = -\rho g = -\frac{M_\mathrm{a} g p}{RT}, \text{ or } p(z) = p_0 \left(1 - \frac{Lz}{T_0}\right)^{0.03417/L} \text{ [kPa]}, \quad gM_\mathrm{a}/R = 0.03417$$
$$\rho(z) = \rho_0 \left(1 - \frac{Lz}{T_0}\right)^{(0.03417/L-1)} \text{ [kg m}^{-3}\text{]} \tag{49}$$

Using the above relations, we can determine the thermodynamic properties of the atmosphere for any altitude. The most important effect is the change in air humidity with the corresponding evaporation (latent) heat of water $h_\mathrm{lv} = 2264\,\mathrm{kJkg}^{-1}$.

Heat supplied by solar radiation increases the amount of water vapour above the ocean $T\mathrm{d}s = h_\mathrm{lv}\mathrm{d}w_\mathrm{v}$, and the balance of momentum (26) can be written as

$$T\frac{\partial s}{\partial r} + 2r\omega_\mathrm{z}^2 = h_\mathrm{vl}\frac{w_\mathrm{v}}{\partial r} + 2r\omega^2 = \frac{\partial h_\mathrm{t}}{\partial r} \tag{50}$$

After integration from $r = 0$ to the edge of the solid body vortex R_max, where the maximum circumferential velocity $v_{\varphi,\mathrm{max}}$) is reached, we obtain

$$\Delta h_\mathrm{t} = h_{\mathrm{t},\,R_\mathrm{max}} - h_{\mathrm{t},0} = h_\mathrm{vl}(w_{\mathrm{v},\,R_\mathrm{max}} - w_{\mathrm{v},\,0}) + v_{\varphi,\,\mathrm{max}}^2, \quad \text{for } v_{\varphi,\,\mathrm{max}} = R_\mathrm{max}\omega_\mathrm{z}. \tag{51}$$

Thus, in the case of a flow field in the form of a solid vortex, the total enthalpy increases during evaporation $h_\mathrm{vl} > 0$. The amount of vapour ρ_v increases radially outwards. Thus, the total energy of tropical cyclones

and twisters increases with the evaporation of water due to solar activity. However, in the potential part of the vortex, the total enthalpy decreases, which also follows from Eq. (50)

$$\frac{\partial h_\mathrm{t}}{\partial r} = T\frac{\partial s}{\partial r} = h_\mathrm{vl}\frac{\partial w_\mathrm{v}}{\partial r} \tag{52}$$

which yields after integration from R_max to $r_2 \gg R_\mathrm{max}$

$$h_{\mathrm{t},\,r_2} - h_{\mathrm{t},\,R_\mathrm{max}} = h_\mathrm{vl}\big(w_{\mathrm{v},\,r_2} - w_{\mathrm{v},\,R_\mathrm{max}}\big) \quad \text{for } v_\varphi = \frac{\omega_\mathrm{z} R_\mathrm{max}^2}{r},\ r > R_\mathrm{max} \tag{53}$$

The total enthalpy h_{t,r_2} at the outer edge of the potential vortex is because of condensation less than at the edge of the eye, i.e. $w_{\mathrm{v},\,r_2} \ll w_{\mathrm{v},\,R_\mathrm{max}}$. Tropical cyclones are accompanied by rain at their outer edges [15,18]. Using the sum of Eqs. (51), (53) we eliminate the term $h_\mathrm{lv} w_{\mathrm{l},\,R_\mathrm{max}}$ and get the relation for the maximum velocity of moist air at the outer boundary of the cyclone eye

$$v_{\varphi,\,\mathrm{max}}^2 = h_\mathrm{vl}(w_{\mathrm{v},\,0} - w_{\mathrm{v},\,r_2}) + h_{\mathrm{t},\,r_2} - h_{\mathrm{t},\,0}, \quad \text{for } v_{\varphi,\,\mathrm{max}} = \omega_\mathrm{z} R_\mathrm{max} \tag{54}$$

Dissipative processes caused by viscosity and thermal conductivity of air were neglected in deriving this relationship, resulting in a high velocity value. For this reason, the result is more qualitative. Nevertheless, it follows that the cyclone disappears under the following conditions

$$w_{\mathrm{t},\,0} \to w_{\mathrm{t},\,r_2}, \quad \text{and} \quad h_{\mathrm{t},\,r_2} - h_{\mathrm{t},\,0} = c_\mathrm{p}(T_{\mathrm{r}_2} - T_0) \to 0, \ \text{for } r_2 \to \infty. \tag{55}$$

This usually happens when the cyclone leaves the ocean and travels over land, such that the rising moist air disappears. If we take the experimentally determined maximum speed $v_{\varphi\ \mathrm{max}} = 62\,\mathrm{m/s}$ for $R_\mathrm{max} = 32\,\mathrm{km}$, [15] we can calculate the circulation (30) on the outer edge of the eye of the cyclone $\Gamma = \omega_\mathrm{z} R_\mathrm{max}^2 = 1.984 \cdot 10^6\,\mathrm{m^2\,s^{-1}}$, where $\omega_\mathrm{z} = 1.94 \cdot 10^{-3}\,\mathrm{s^{-1}}$, see Fig. 8. Equation (54) can be evaluated for the following two extreme cases:

- The temperature in the core of the cyclone eye is the same as at its edge, i.e. $T_0 = T_{\mathrm{r}_2}$ then the water content of the air in the eye is greater, specifically $w_{\mathrm{v},\,0} = w_{\mathrm{v},\,r_2} + 0.0017$
- The water content of the air in the core of the eye is the same as at its edge, i.e. $w_{\mathrm{v},\,0} = w_{\mathrm{v},\,r_2}$ leading to a higher temperature at the edge, specifically $T_{r_2} = T_0 + 3.8\,\mathrm{K}$

This qualitative estimate neglects the strong influence of dissipative processes (turbulence at the Earth's surface), and the potential vortex is not fully developed, similar to a vortex tube, see Figs. 3 and 4. It follows that the cyclone is maintained by an imbalance of humidity and/or temperature, or a combination of both. Nevertheless, it follows that the air inside the vortex must contain more vapour than the air at the far edge of the vortex.

The existence of a cyclone is not possible without the vertical flow of wet air. Provided that the partial pressure of water vapour is much less than the partial pressure of air, i.e. for $p_\mathrm{v} \to 0 \ll p_\mathrm{a}$, from Eq. (46) results that the moist air has less density than dry air, specifically $\rho \doteq \rho_\mathrm{a}\,[1 + (M_\mathrm{a}/M_\mathrm{v} - 1)\,w_\mathrm{v}]^{-1}$. The vertical movement of moist air is induced by buoyancy, and its speed can be estimated from the balance of momentum

$$\frac{1}{2}\frac{\mathrm{d}v_\mathrm{z}^2}{\mathrm{d}z} = \underbrace{-\frac{1}{\rho}\frac{\partial p}{\partial z} - g}_{=0,\ \text{see (49)}} - \left(1 - \frac{\rho_\mathrm{a}}{\rho}\right) = g\left(\frac{M_\mathrm{a}}{M_\mathrm{v}} - 1\right) w_\mathrm{v} \tag{56}$$

The specific humidity $w_\mathrm{v}(z)$ only depends on the temperature $T(z)$ from Eq. (49) and decreases with altitude, similar to the saturated vapour pressure (48) [12]

$$\mathrm{d}w_\mathrm{v}(z) = -\beta w_\mathrm{v}(z)\mathrm{d}z, \quad \text{or } w_\mathrm{v}(z) = w_\mathrm{v}(0)\exp(-\beta(z - z_0)) \ \text{for } \beta \simeq 3.77 \cdot 10^{-4}\,[\mathrm{m^{-1}}] \tag{57}$$

Here, the magnitude of the coefficient β is approximated and serves to estimate the dependency of the vertical velocity of moist air on the altitude. We introduce this dependence in Eq. (56). After integration in the range $(0,\ z)$ we get

$$v_\mathrm{z}(z) = \sqrt{\left(\frac{M_\mathrm{a}}{M_\mathrm{v}} - 1\right)\frac{2g w_\mathrm{v}(0)}{\beta}}\left[1 - \exp(-\beta z)\right]^{1/2}, \quad \text{for } v_\mathrm{z}(0) = 0 \tag{58}$$

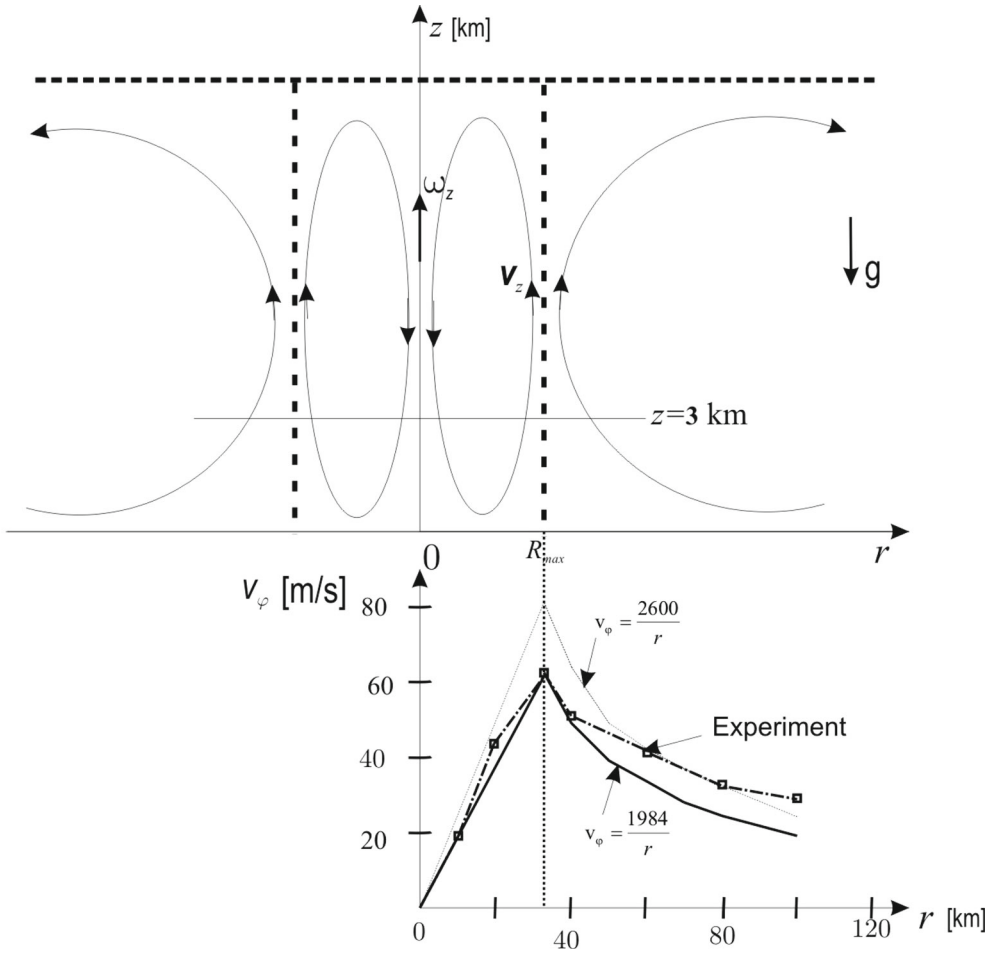

Fig. 8 Comparison of a qualitative analysis of cyclone dynamics with experimental results presented in the more detailed analysis [15]. Values for determining the potential vortex circulation Γ (12), were taken from the experiment [15], i.e. $\Gamma = v_{\varphi,\max} R_{\max} = 1984$. $\Gamma = 2600$ was used to demonstrate better fitting of the experiment

This formula gives a speed of $v_z = 20.7\mathrm{m/s}$ at an altitude of $z = 3\,\mathrm{km}$ for specific humidity at the ocean level $w_v(0) = 0.02$. It should be taken into account that at high altitudes water vapour is supersaturated $p_v/p_{sat} > 1$ and condensation occurs. As a result, the air flow is inhibited. The magnitude of air deceleration with condensation can be estimated from the total enthalpy (5)

$$\dot{h}_t = c_p \dot{T} + \dot{\frac{v_z^2}{2}} + g\dot{z} = T\dot{s} + \frac{1}{\rho}\frac{\partial p}{\partial t}\bigg|_z \tag{59}$$

In case the atmosphere is in a steady state ($\partial p/\partial t|_z = 0$), a parcel of a moist air at high altitude is slowed down according to the relationship

$$\dot{v}_z = c_p \left[\frac{h_{lv}}{c_p}\frac{\mathrm{d}w_v}{\mathrm{d}z} - \underbrace{\left(\frac{\mathrm{d}T}{\mathrm{d}z} + \frac{g}{c_p}\right)}_{=0 \text{ for dry air}} \right] \approx h_{lv}\frac{\mathrm{d}w_v(z)}{\mathrm{d}z} < 0 \tag{60}$$

For example, at an altitude of 10 km, the decrease in relative humidity is $\mathrm{d}w/\mathrm{d}z = 1.74 \times 10^{-6}\mathrm{m}^{-1}$, and the corresponding deceleration is $\dot{v}_z = -4.5\,\mathrm{m\,s}^{-2}$.

6 Conclusion

In spite of the huge amount of publication concerning the Ranque–Hilsch effect and many experiments, which proved its actual function, its physical origin is still under discussion [25]. Theoretical analysis supported by experiments and numerical simulations provided a large amount of partial knowledge. These findings can be satisfactorily unified by using the properties of total enthalpy. The important role of the total enthalpy for inviscid flow followed from the variational analysis [22,27]. The use of total enthalpy offers a more general view on the stability of flow of viscous fluids. Moreover, the thermodynamic criteria of stability of the steady state and the stability of the processes are applied to specific cases.

This theory was verified for all modifications of the Couette flow, even for a solid body rotation, where the Rayleigh condition failed. It was shown that the solid body vortex is at the margin of stability, which is experimentally observed. Analogously, the potential vortex is stable in the case of the thermodynamic criterion and plays an important role in clarifying the function of the vortex tube. These conclusions can even be applied to processes in the atmosphere (estimation of the power of hurricanes and tornadoes [18]). The increase in total enthalpy caused by the evaporation of water in the inner part of a tropical cyclone (solid body vortex) and the decrease of enthalpy in its outer part (potential vortex) leads to great stability and long persistence of this atmospheric phenomenon.

Acknowledgements We gratefully acknowledge the support of the Grant Agency of the Czech Republic-Czech Science Foundation (Project No. 21-26232J) and the institutional support RVO: 61388998. Moreover, we kindly acknowledge the funding of this work by the German Research Foundation (DFG) (Grant No. WE 2549/38, Project No. 363548659) and the Sino-German Center for Research Promotion (Grant No. GZ 1577).

Open Access This article is licensed under a Creative Commons Attribution 4.0 International License, which permits use, sharing, adaptation, distribution and reproduction in any medium or format, as long as you give appropriate credit to the original author(s) and the source, provide a link to the Creative Commons licence, and indicate if changes were made. The images or other third party material in this article are included in the article's Creative Commons licence, unless indicated otherwise in a credit line to the material. If material is not included in the article's Creative Commons licence and your intended use is not permitted by statutory regulation or exceeds the permitted use, you will need to obtain permission directly from the copyright holder. To view a copy of this licence, visit http://creativecommons.org/licenses/by/4.0/.

Funding Open access publishing supported by the National Technical Library in Prague.

Declarations

Conflict of interest The authors declare that they have no conflict of interest.

References

1. Antošová, Z., Trávníček, Z.: Control of annular air jet by means of swirling effect. In: 10th International Symposium on Turbulence, Heat and Mass transfer, THMT-23, Rome, Sept. 11–15, pp. 123–126 (2023)
2. Batchelor, G.K.: An Introduction to Fluid Mechanics. Cambridge University Press, Cambridge (2000)
3. Biegger, C., Weigland, B.: Flow and heat transfer measurements in a swirl chamber with different outlet geometries. Exp. Fluids **56**, 78 (2015). https://doi.org/10.1007/s00348-015-1937-3
4. Biegger, C., Sotgiu, C., Weigand, B.: Numerical investigation of flow and heat transfer in a swirl tube. Int. J. Therm. Sci. (2014). https://doi.org/10.1016/j.ijthermalsci.2014.12.001
5. Chandrasekhar, S.: Hydrodynamic and Hydromagnetic Stability. Clarendon, Oxford (1961)
6. Dmitrenko, A.V.: Theoretical calculation of the laminar-turbulent transition in the round tube on the basis of stochastic theory of turbulence and equivalence of measures. Continuum Mech. Thermodyn. **34**, 1375–1392 (2022). https://doi.org/10.1007/s00161-022-01125-4
7. Dostalík, M., Průša, V., Rajagopal, K.R.: Unconditional finite amplitude stability of a fluid in a mechanically isolated vessel with spatially non-uniform wall temperature. Continuum Mech. Thermodyn. **33**, 515–543 (2021). https://doi.org/10.1007/s00161-020-00925-w
8. de Groot, S.R., Mazur, P.: Non-equilibrium Thermodynamics. North-Holland, Amsterdam (1962)
9. Escudier, M.P., Bornstein, J., Maxworthy, T.: The dynamics of confined vortices. Proc. R. Soc. Lond. A **382**, 335–360 (1982). https://doi.org/10.1098/rspa.1982.0105
10. Eskinazi, S.: Fluid Mechanics and Thermodynamics of Environment. Academic Press, New York (1975). https://doi.org/10.1016/B978-0-12-242540-0.X5001-X
11. Glansdorff, P., Prigogine, I.: Thermodynamic Theory of Structure, Stability and Fluctuations. Wiley, New York (1971)
12. Hartmann, D.L.: Global Physical Climatology, 2nd edn. Elsevier, Amsterdam (2016). https://doi.org/10.1016/C2009-0-00030-0
13. Hilsch, R.: The use of the expansion of gases in a centrifugal field as cooling process. Rev. Sci. Instrum. **18**(2), 108–1113 (1947). https://doi.org/10.1063/1.1740893. (**translation of an article in Zeit. Naturwis. 1 208**)

14. Jou, D., Casas-Vázquez, J., Lebon, G.: Extended Irreversible Thermodynamics, 4th edn. Springer, Berlin (2010)
15. Kerry, A.E.: Tropical cyclone energetics and structure. Atmos. Turbul. Mesoscale Meteorol. **165**, 192 (2004)
16. Landau, L.D., Lifshitz, E.M.: Statistical Physics. Pergamon Press, Oxford (1980)
17. Landau, L.D., Lifshitz, E.M.: Fluid Mechanics. Pergamon Press, Oxford (1987)
18. Lighthill, J.: Fluid mechanics of tropical cyclones. Theor. Comput. Fluid Dyn. **10**, 3–21 (1998)
19. Maršík, F.: Consequences of thermodynamical conditions of stability for thermoviscous fluids and thermoviscoelastic solids. Acta Phys. Hung. **66**(1–4), 195–202 (1989). https://doi.org/10.1007/BF03155792
20. Maršík, F.: Continuum Thermodynamics. Academia, Praha (1999). (**in Czech, Termodynamika kontinua**)
21. Maršík, F., Trávníček, Z., Novotný, P., Werner, E.: Stability of swirling annular flow. J. Flow Vis. Image Process. **17**(3), 267–279 (2010). https://doi.org/10.1615/JFlowVisImageProc.v17.i3.70
22. Marsik, F., Novotny, P.: Variational formulation of continuum mechanics based on the Lagrangian with the friction force. In: Bai, Y., Wang, J., Fang, D. (eds.) Proceedings of the XXIII ICTAM on CD-ROM, 19–24 August 2012, pp. 69–70. China Science Literature Publishing House, Beijing (2012)
23. Seibold, F., Weigand, B., Marsik, F., Novotny, P.: Thermodynamic stability condition of swirling flows in convergent vortex tubes. In: Proceedings of the International Gas Turbine Congress 2019 Tokyo (2019) https://www.researchgate.net/publication/342122926
24. Seibold, F., Weigand, B.: Numerical analysis of the flow pattern in convergent vortex tubes for cyclone cooling applications. Int. J. Heat Fluid Flow **90**, 108806 (2021). https://doi.org/10.1016/j.ijheatfluidflow.2021.108806
25. Seibold, F., Ligrani, P., Weigand, B.: Flow and heat transfer in swirl tubes—a review. Int. J. Heat Mass Transf. **187**, 122455 (2022). https://doi.org/10.1016/j.ijheatmasstransfer.2021.122455
26. Spalart, P.R., Deck, S., Shur, M.L., Squires, K.D., Strelets, MKh., Travin, A.: A new version of detached Eddy simulation, resistant to ambiguous grid densities. Theor. Comput. Fluid Dyn. **20**, 181–195 (2006). https://doi.org/10.1007/s00162-006-0015-0
27. Seliger, R.L., Whitham, G.B.: Variational principles of continuum mechanics. Proc. R. Soc. A **305**, 1–25 (1968)
28. Taylor, G.I.: Stability of a viscous liquid contained between two rotating cylinders. Philos. Trans. R. Soc. Lond. A **223**, 289–343 (1923). https://doi.org/10.1098/rsta.1923.0008

Publisher's Note Springer Nature remains neutral with regard to jurisdictional claims in published maps and institutional affiliations.